Identify dominant dimensions of 3D hand shapes using statistical shape model and deep neural network

Yang, Yusheng; Zhou, Hongpeng; Song, Yu; Vink, Peter

DOI
10.1016/j.apergo.2021.103462

Publication date
2021

Document Version
Final published version

Published in
Applied Ergonomics

Applied Ergonomics 96 (2021) 103462

Contents lists available at ScienceDirect

Applied Ergonomics

journal homepage: www.elsevier.com/locate/apergo

Identify dominant dimensions of 3D hand shapes using statistical shape model and deep neural network

Yusheng Yang [a,b], Hongpeng Zhou [c], Yu Song [b,*], Peter Vink [b]

[a] School of Mechatronic Engineering and Automation, Shanghai University, Shanghai, 200444, China
[b] Faculty of Industrial Design Engineering, Delft University of Technology, Delft, South Holland, 2628CE, the Netherlands
[c] Faculty of Mechanical, Maritime and Materials Engineering, Delft University of Technology, Delft, South Holland, 2628CD, the Netherlands

ARTICLE INFO

Keywords:
Dominant hand dimensions
Measurement stability
Structured sparsity learning

ABSTRACT

Hand anthropometry is one of the fundamentals of ergonomic research and product design. Many studies have been conducted to analyze the hand dimensions among different populations, however, the definitions and the numbers of those dimensions were usually selected based on the experience of the researchers and the available equipment. Few studies explored the importance of each hand dimension regarding the 3D shape of the hand. In this paper, we aim to identify the dominant dimensions that influence the hand shape variability while considering the stability of the measurements in practice. A novel four-step research method was proposed where in the first step, based on literature study, we defined 58 landmarks and 53 dimensions for the exploration. In the second step, 80,000 virtual hand models, each had the associated 53 dimensions, were augmented by changing the weights of Principle Components (PCs) of a statistical shape model (SSM). Deep neural networks (DNNs) were used to establish the inverse relationships from the dimensions to the weight of each PC of the hand SSM. Using the structured sparsity learning method, we identified 21 dominant dimensions that represent 90% of the variance of the hand shape. In the third step, two different manual measuring methods were used to evaluate the stability of the measurements in practice. Finally, we selected 16 dominant dimensions with lower measurement variance by synthesizing the findings in Step 2 and 3. It was concluded that the recognized 21 dominant dimensions can be treated as the reference dimensions for anthropometric study and using the selected 16 dominant dimensions with lower measurement variance, ergonomists are able to generate a 3D hand model based on simple measurement tools with an accuracy of 5.9 mm. Though the accuracy is limited, the efforts are minimum, and the results can be used as an indicator in the early stage of research/design.

1. Introduction

Over the past decades, extensive efforts were paid to investigate the hand anthropometric measures regarding people in different regions, different genders, different age groups, etc., and the collected data was used in different ergonomics studies and product design applications (Harih and Dolšak, 2013), (Yu et al., 2013), (Ahn et al., 2016), (Stellon et al., 2017). For instance, Nag et al. (2003) applied 51 dimensions of the hand in the design of hand tools for Indian women. Yu et al. (2018) analyzed comfort of gloves based on 24 hand dimensions. Shahriar et al. (2020) summarized those application areas as evaluating grip and pinch strength, determining manual dexterity and performance, optimizing grip span, predicting stature, designing prosthesis, determining touch interaction, evaluating phone size and comfort of gloves, and analyzing operations on handheld devices and handles.

Though the anthropometric measures of the hand were essential in those applications (NASA, 1978), (Wagner, 1988a), (Greiner, 1991), the definitions of the dimensions and the measuring methods vary as summarized in Table 1. ISO 7250–1:2017 (International Organization for Standardization, 2017) recommended 62 measurements where 11 are associated with the hand, however the importance of each dimension was not addressed. Furthermore, the recommended dimensions were not always applied due to different constraints. For example, in the anthropometric study of the hand of the Jordanian population, Mandahawi et al. (2008) measured 24 dimensions from 120 females and 115 males, while García-Cáceres et al. (2012) used 33 hand dimensions in the design of manual tools for Colombian floriculture.

Besides the definitions of the dimensions, using different tools and

* Corresponding author.
E-mail address: y.song@tudelft.nl (Y. Song).

https://doi.org/10.1016/j.apergo.2021.103462
Received 25 February 2021; Received in revised form 30 April 2021; Accepted 11 May 2021
Available online 25 May 2021

methods to gather correct hand anthropometric measurements can also be challenging due to the involuntary movement of the hand and the deformation of the soft tissue. According to whether the measuring tool (s) is in contact with the hand or not, the measurement methods can be categorized to direct and indirect methods. Tape measures, calipers, and rulers are often used to directly obtain the hand dimensions. However, the deformation of the soft tissue is inevitable in the use of the direct methods, and relatively large inter- and intra-observer variations were often observed (Bennett and Osborne, 1986). The indirect methods utilize 2D photography and 3D scanning technologies to overcome the disadvantages of using the direct method (Yu et al., 2013), (Patel et al., 2018). For instance, Ozsoy et al. (2009) found that using 3D scanning was a robust and easy way to obtain the precise measurement of the hand. However, it is more expensive regarding both the equipment and the needed manpower.

In summary, though many hand dimensions were defined and used in different applications, the definition of hand dimensions and the selection of measurement methods were often prone to the experience of the researcher(s) and limited by practical constraints. Researchers and industries ask for a more effective and efficient method for collecting hand anthropometric data for different applications. One way to answer this question is to identify the importance of each dimension regarding the 3D shape of the human hand and use a prioritized list to accelerate the data acquisition process. However, only a few studies discussed the contribution of each dimension to the 3D hand shape. For instance, in a hand anthropometric survey, Jee and Yun (2016) analyzed data collected from 321 subjects in Korean, and identified that the hand breadth, the palm length, and the finger length these three factors can describe 78.3% of the variance of the hand shape. However, only 27 hand dimensions were studied in the study.

Advancement in computer science offers new opportunities in exploring the importance of dimensions of the human hand, regarding both the amount of data and the relations between the dimensions and the shape. For instance, using a hand SSM (Yang et al., 2021), the 3D hand shape can be described with a set of weights regarding the corresponding principal components (PCs), and a new hand model can be augmented based on a linear combination of the weights and the corresponding PCs. For exploring relations between data and known labels, the deep neural network (DNN) is a prevalent modeling tool and showed excellent performance in many applications, e.g. image classification (Krizhevsky et al., 2012), language recognition (Richardson et al., 2015), system identification (Sjöberg et al., 1994) (Hochreiter and Urgen Schmidhuber, 1997) (Zhou et al., 2019a) and pattern recognition (Bishop, 2006). Using DNNs, the relations from the anthropometric dimensions to the weights of PCs of an SSM might be established, and the importance of different anthropometric dimensions can be further explored using the network compression method (Cheng et al., 2017), where insignificant inputs, e.g. hand dimensions, of a DNN can be pruned while the performance of the DNN will not decrease significantly.

In this paper, we developed a new strategy to identify the dominant hand dimensions regarding the 3D hand shape and try to establish the relations from those dimensions to 3D shapes. The scientific contributions of this paper are:

1. Combing the computational methods and the traditional measurement methods, we proposed a novel approach for identifying dominant dimensions of the hand;
2. Using a hand SSM and the DNN, we modeled the relations from human hand anthropometric dimensions to weights of the PCs of the SSM, and highlighted the importance of different dimensions regarding 3D shape, respectively;
3. Using direct and indirect measurement methods, we analyzed the stability of the anthropometric measurements regarding different dimensions of the human hand;
4. Based on the synthesis of these results, we proposed a set of dominant dimensions with a low measurement variance (DDLMVs), and a 3D hand shape approximation method based on these dimensions.

2. Materials and method

Fig. 1 presents an overview of the proposed approach, which can be divided to four steps: First we proposed a set of dimensions of the hand based on the synthesis of the specified dimensions in the literature. Secondly, 80,000 3D hand models with landmarks and dimensions were augmented using a posture invariant hand SSM. Using DNN models, the

Table 1
Literature on anthropometry of (or related to) the human hand.

Reference	Number of dimensions (related to hand)	Number of subjects	Target population	Measurement target	Measurement method	Year
NASA (NASA, 1978)	295 (16)	61 populations	USA, Europe and Asia	Body	Direct method	1978
Wagner (Wagner, 1988a)	20	238	28 countries	Hand	Direct method	1988
Greiner et al. (Greiner, 1991)	86	2307	American	Hand	Direct method and indirect method	1991
Robinette et al. (Robinetteet al., 1991)	99 (2)	4431	Europe and North America	Body	Indirect method	1991
Kar et al. (Kar et al., 2003)	8	404	Indian	Hand	Direct method	2003
Nag et al. (Nag et al., 2003)	51	95	Indian	Hand	Direct method	2003
Cakit et al. (Cakit et al., 2006)	33	165	Turkish	Hand	Direct method	2006
ISO 7250–1 (International Organization for Standardization, 2017)	62 (11)	N/A	N/A	Body	Direct method and indirect method	2008
Chuan et al. (Chuan et al., 2010a)	36 (2)	Indonesia:377 Singapore:315	Singaporean, Indonesian	Body	Direct method	2010
Chandra et al. (Chandra et al., 2011)	37	878	Indian	Hand	Direct method	2011
Yu et al. (Yu et al., 2013)	33	10	N/A	Hand	Direct method and indirect method	2013
Khadem et al. (Khadem and Islam, 2014a)	37 (6)	470	Bangladeshi	Body	Direct method	2014
Bures et al. (Bures et al., 2016)	8	1032	Czechs	Hand	Direct method	2016
Jee and Yun (Jee and Yun, 2016)	21	321	South Korean	Hand	Direct method and indirect method	2016
Vergara et al. (Vergara et al., 2018)	99	139	Spanish	Hand	Direct method and indirect method	2018
Rhiu and Kim (Rhiu and Kim, 2019)	19	172	South Korean	Hand	Direct method	2019
Yu et al. (Yu et al., 2018)	24	30	Hong Kongese	Hand	Direct method and indirect method	2019

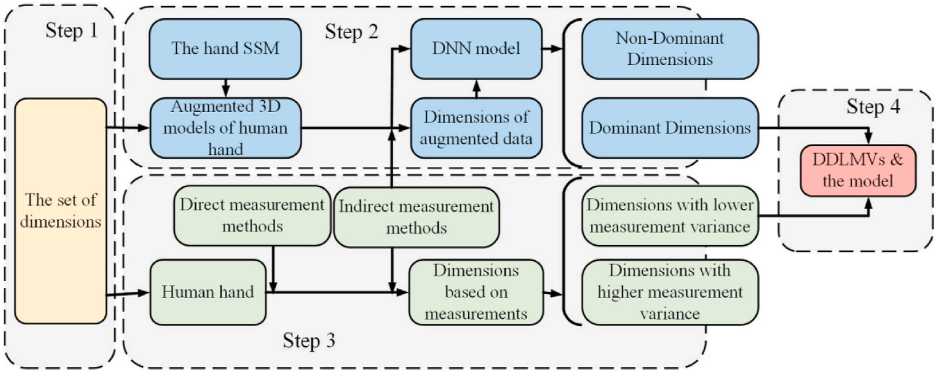

Fig. 1. An overview of the proposed approach.

relations from the dimensions to the 3D models were built. Further analysis of the inputs of DNN models revealed that those dimensions can be categorized as Dominant Dimensions and Non-Dominant Dimensions, based on the contribution of each dimension to the 3D shape. Thirdly, to investigate the robustness of the measurement methods, we measured the same dimensions using both direct and indirect methods and categorized those dimensions as Dimensions with lower measurement variance (DLMV) and Dimensions with higher measurement variance (DHMV). Finally, based on the Dominant Dimensions generated from Step 2 and DLMV in Step 3, we proposed a list of 16 DDLMVs and built a DNN model which is able to generate 3D hand models using these DDLMVs.

2.1. Hand dimensions

Based on literatures, we summarized 58 landmarks and 53 dimensions on the human hand (Fig. 2) as the starting point of the exploration. In this study, all dimensions were measured in the palmar aspect and those dimensions were defined based on the "standard posture", where the palm is kept flat with wide spread fingers. Table 2

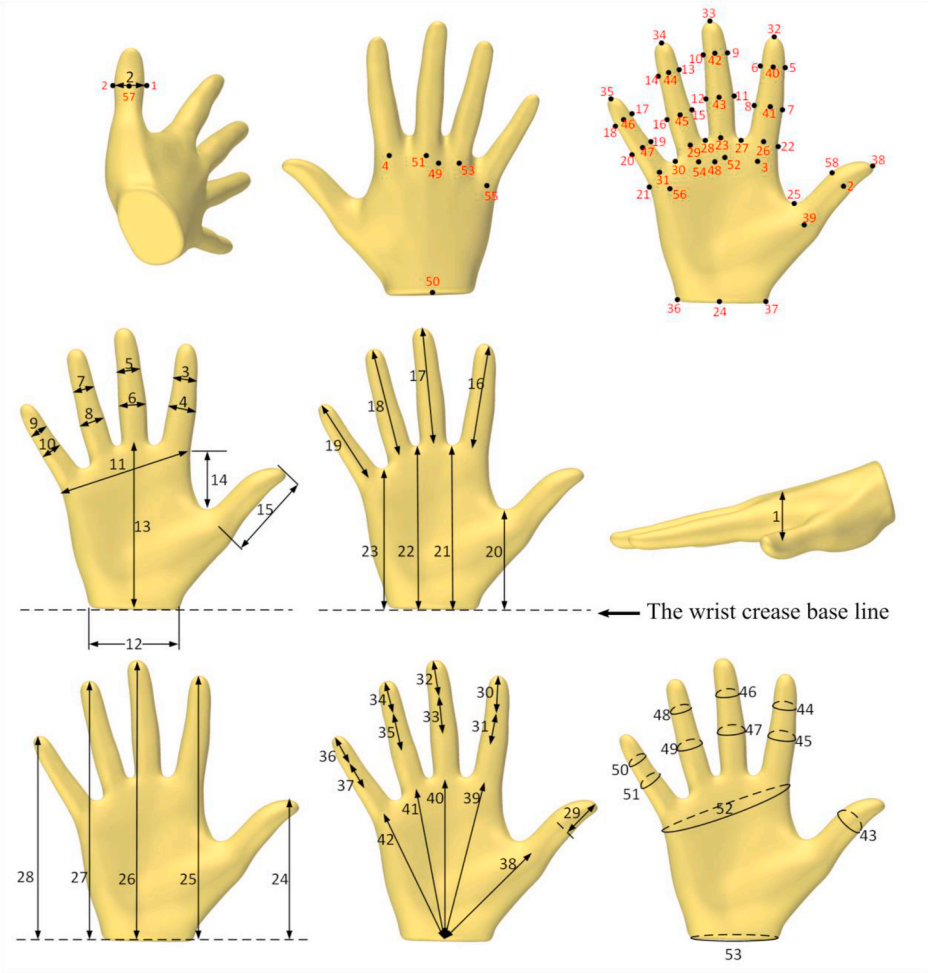

Fig. 2. The definition of the landmarks (red) and dimensions (black). (For interpretation of the references to color in this figure legend, the reader is referred to the Web version of this article.)

Table 2
Definition of hand dimensions.

Name	Dimension	Landmarks	Projected	References
D1	Hand thickness (maximum thickness across the knuckles)	Knuckle 1: From 3 to 4 Knuckle 2: From 51 to 52 Knuckle 3: From 53 to 54 Knuckle 4: From 55 to 56	N	(Churchill et al., 1978), (International Organization for Standardization, 2017), (Greiner, 1991), (Jee and Yun, 2016), (García-Cáceres et al., 2012), (Cakit et al., 2014), (Dewangan et al., 2008), (GARRETT, 1971), (Imrhan et al., 1993), (Imrhan et al., 2009), (Kar et al., 2003), (Mandahawi et al., 2008), (Nag et al., 2003), (Nag et al., 2003), (Okunribido, 2000), (Stephanidis, 2014), (Chandra et al., 2011), (Garrett, 1971)
D2	Digit 1 interphalangeal joint breadth	From 1 to 2	N	(International Organization for Standardization, 2017) (Greiner, 1991) (Jee and Yun, 2016) (García-Cáceres et al., 2012) (GARRETT, 1971) (Nag et al., 2003) (Garrett, 1971), (Vergara et al., 2018)
D3	Digit 2 distal interphalangeal joint breadth	From 6 to 5	Y	(International Organization for Standardization, 2017) (Greiner, 1991) (García-Cáceres et al., 2012) (Cakit et al., 2014) (GARRETT, 1971) (Nag et al., 2003) (Garrett, 1971) (Vergara et al., 2018), (Robinette and Annis, 1986)
D4	Digit 2 proximal interphalangeal joint breadth	From 8 to 7	Y	(International Organization for Standardization, 2017) (Greiner, 1991) (Jee and Yun, 2016) (García-Cáceres et al., 2012) (Cakit et al., 2014) (GARRETT, 1971) (Nag et al., 2003) (Garrett, 1971) (Vergara et al., 2018) (Robinette and Annis, 1986)
D5	Digit 3 distal interphalangeal joint breadth	From 10 to 9	Y	(Greiner, 1991) (García-Cáceres et al., 2012) (Cakit et al., 2014) (GARRETT, 1971) (Imrhan et al., 1993) (Imrhan et al., 2009) (Mandahawi et al., 2008) (Nag et al., 2003) (Okunribido, 2000) (Chandra et al., 2011) (Garrett, 1971) (Vergara et al., 2018) (Robinette and Annis, 1986)
D6	Digit 3 proximal interphalangeal joint breadth	From 12 to 11	Y	(Churchill et al., 1978) (Greiner, 1991) (Jee and Yun, 2016) (García-Cáceres et al., 2012) (Cakit et al., 2014) (GARRETT, 1971) (Imrhan et al., 1993) (Imrhan et al., 2009) (Mandahawi et al., 2008) (Nag et al., 2003) (Okunribido, 2000) (Chandra et al., 2011) (Garrett, 1971) (Vergara et al., 2018) (Robinette and Annis, 1986)
D7	Digit 4 distal interphalangeal joint breadth	From 14 to 13	Y	(Greiner, 1991) (Cakit et al., 2014) (Garrett, 1971) (Vergara et al., 2018) (Robinette and Annis, 1986)
D8	Digit 4 proximal interphalangeal joint breadth	From 16 to 15	Y	(Greiner, 1991) (Jee and Yun, 2016) (Cakit et al., 2014) (Garrett, 1971) (Vergara et al., 2018) (Robinette and Annis, 1986)
D9	Digit 5 distal interphalangeal joint breadth	From 18 to 17	Y	(Greiner, 1991) (Cakit et al., 2014) (Imrhan et al., 1993) (Imrhan et al., 2009) (Mandahawi et al., 2008) (Okunribido, 2000) (Chandra et al., 2011) (Garrett, 1971) (Vergara et al., 2018) (Robinette and Annis, 1986)
D10	Digit 5 proximal interphalangeal joint breadth	From 20 to 19	Y	(Greiner, 1991) (Jee and Yun, 2016) (Cakit et al., 2014) (Imrhan et al., 1993) (Imrhan et al., 2009) (Mandahawi et al., 2008) (Okunribido, 2000) (Chandra et al., 2011) (Garrett, 1971) (Vergara et al., 2018) (Robinette and Annis, 1986)
D11	Palm breadth	From 21 to 22	Y	(Churchill et al., 1978) (International Organization for Standardization, 2017) (Greiner, 1991) (Jee and Yun, 2016) (García-Cáceres et al., 2012) (Cakit et al., 2014) (Dewangan et al., 2008) (GARRETT, 1971) (Imrhan et al., 1993) (Imrhan et al., 2009) (Kar et al., 2003), (Mandahawi et al., 2008) (Nag et al., 2003) (Okunribido, 2000) (Stephanidis, 2014) (Chandra et al., 2011) (Garrett, 1971) (Robinette and Annis, 1986), (Wagner, 1988b), (Yu et al., 2013), (Hertzberg, 1912), (Klamklay et al., 2008), (Prado-León et al., 2001), (Bures et al., 2016), (Bayraktar and Özşahin, 2018), (Kanchan and Krishan, 2011), (Chuan et al., 2010b) (Khadem and Islam, 2014b)
D12	Wrist breadth	From 36 to 37	Y	(Churchill et al., 1978) (Greiner, 1991) (Jee and Yun, 2016) (García-Cáceres et al., 2012) (Cakit et al., 2014) (GARRETT, 1971) (Nag et al., 2003) (Stephanidis, 2014) (Garrett, 1971) (Wagner, 1988b) (Yu et al., 2013)
D13	Palm length	From 33 to wrist crease base line	Y	(Churchill et al., 1978) (International Organization for Standardization, 2017) (Greiner, 1991) (Jee and Yun, 2016) (Dewangan et al., 2008) (Kar et al., 2003) (Wagner, 1988b) (Yu et al., 2013) (Prado-León et al., 2001) (Bures et al., 2016) (Kanchan and Krishan, 2011)
D14	Length of root of index finger to the root of thumb	From 22 to 25	Y	(Churchill et al., 1978) (Yu et al., 2013), (Yu et al., 2018)
D15	Digit 1 length	From 38 to 39	Y	(International Organization for Standardization, 2017) (Greiner, 1991) (Jee and Yun, 2016) (García-Cáceres et al., 2012) (Cakit et al., 2014) (GARRETT, 1971) (Nag et al., 2003) (Okunribido, 2000) (Garrett, 1971) (Robinette and Annis, 1986) (Yu et al., 2013) (Bures et al., 2016) (Yu et al., 2018), (Harih and Dolšak, 2014)
D16	Digit 2 length	From 32 to 26	Y	(International Organization for Standardization, 2017) (Greiner, 1991) (Jee and Yun, 2016) (García-Cáceres et al., 2012) (Cakit et al., 2014) (GARRETT, 1971) (Nag et al., 2003) (Stephanidis, 2014) (Garrett, 1971) (Wagner, 1988b) (Yu et al., 2013) (Bures et al., 2016) (Yu et al., 2018)
D17	Digit 3 length	From 33 to 23	Y	(Greiner, 1991) (Jee and Yun, 2016) (García-Cáceres et al., 2012) (Cakit et al., 2014) (GARRETT, 1971) (Imrhan et al., 1993) (Imrhan et al., 2009) (Mandahawi et al., 2008) (Nag et al., 2003) (Okunribido, 2000) (Stephanidis, 2014) (Chandra et al., 2011) (Garrett, 1971) (Wagner, 1988b) (Yu et al., 2013) (Bures et al., 2016) (Yu et al., 2018)
D18	Digit 4 length	From 34 to 29	Y	(Greiner, 1991) (Jee and Yun, 2016) (García-Cáceres et al., 2012) (Cakit et al., 2014) (GARRETT, 1971) (Nag et al., 2003) (Stephanidis, 2014) (Garrett, 1971) (Wagner, 1988b) (Yu et al., 2013) (Yu et al., 2018)
D19	Digit 5 length	From 35 to 31	Y	(Greiner, 1991) (Jee and Yun, 2016) (García-Cáceres et al., 2012) (Cakit et al., 2014) (GARRETT, 1971) (Imrhan et al., 1993) (Imrhan et al., 2009) (Mandahawi et al., 2008) (Nag et al., 2003) (Okunribido, 2000) (Stephanidis, 2014) (Chandra et al., 2011) (Garrett, 1971) (Wagner, 1988b) (Yu et al., 2013) (Yu et al., 2018)
D20	Digit 1 crotch height	From 25 to wrist crease base line	Y	(Greiner, 1991) (Garrett, 1971) (Robinette and Annis, 1986)
D21	Digit 2 crotch height	From 27 to wrist crease base line	Y	(Greiner, 1991) (Garrett, 1971) (Robinette and Annis, 1986)

(*continued on next page*)

Table 2 (*continued*)

Name	Dimension	Landmarks	Projected	References
D22	Digit 3 crotch height	From 28 to wrist crease base line	Y	(Greiner, 1991) (Garrett, 1971) (Robinette and Annis, 1986)
D23	Digit 4 crotch height	From 30 to wrist crease base line	Y	(Greiner, 1991) (Garrett, 1971) (Robinette and Annis, 1986)
D24	Digit 1 height	From 38 to wrist crease base line	Y	(Greiner, 1991) (García-Cáceres et al., 2012) (GARRETT, 1971) (Nag et al., 2003) (Garrett, 1971)
D25	Digit 2 height	From 32 to wrist crease base line	Y	(Greiner, 1991) (García-Cáceres et al., 2012) (GARRETT, 1971) (Nag et al., 2003) (Garrett, 1971) (Yu et al., 2013) (Harih and Dolšak, 2014)
D26	Digit 3 height	From 33 to wrist crease base line	Y	(Churchill et al., 1978) (International Organization for Standardization, 2017) (Greiner, 1991) (Jee and Yun, 2016) (García-Cáceres et al., 2012) (Cakit et al., 2014) (Dewangan et al., 2008) (GARRETT, 1971) (Imrhan et al., 1993) (Imrhan et al., 2009) (Kar et al., 2003) (Mandahawi et al., 2008) (Nag et al., 2003) (Okunribido, 2000) (Stephanidis, 2014) (Garrett, 1971) (Vergara et al., 2018) (Robinette and Annis, 1986) (Wagner, 1988b) (Yu et al., 2013) (Klamklay et al., 2008) (Prado-León et al., 2001) (Bures et al., 2016) (Bayraktar and Özşahin, 2018) (Kanchan and Krishan, 2011) (Chuan et al., 2010b) (Khadem and Islam, 2014b) (Harih and Dolšak, 2014), (Robinette et al., 1999)
D27	Digit 4 height	From 34 to wrist crease base line	Y	(Greiner, 1991) (García-Cáceres et al., 2012) (GARRETT, 1971) (Nag et al., 2003) (Garrett, 1971) (Yu et al., 2013) (Harih and Dolšak, 2014)
D28	Digit 5 height	From 35 to wrist crease base line	Y	(Greiner, 1991) (García-Cáceres et al., 2012) (GARRETT, 1971) (Nag et al., 2003) (Garrett, 1971) (Yu et al., 2013) (Harih and Dolšak, 2014)
D29	Digit 1 distal phalanx link length	From 38 to 2	Y	Greiner (1991)
D30	Digit 2 distal phalanx link length	From 32 to 40	Y	(Greiner, 1991) (Vergara et al., 2018) (Wagner, 1988b) (Harih and Dolšak, 2014)
D31	Digit 2 medial phalanx link length	From 40 to 41	Y	(Greiner, 1991) (Vergara et al., 2018) (Wagner, 1988b)
D32	Digit 3 distal phalanx link length	From 33 to 42	Y	(Greiner, 1991) (Vergara et al., 2018) (Wagner, 1988b) (Harih and Dolšak, 2014)
D33	Digit 3 medial phalanx link length	From 42 to 43	Y	(Greiner, 1991) (Vergara et al., 2018) (Wagner, 1988b)
D34	Digit 4 distal phalanx link length	From 34 to 44	Y	(Greiner, 1991) (Vergara et al., 2018) (Wagner, 1988b)
D35	Digit 4 medial phalanx link length	From 44 to 45	Y	(Greiner, 1991) (Vergara et al., 2018) (Wagner, 1988b)
D36	Digit 5 distal phalanx link length	From 35 to 46	Y	(Greiner, 1991) (Vergara et al., 2018) (Wagner, 1988b)
D37	Digit 5 medial phalanx link length	From 46 to 47	Y	(Greiner, 1991) (Vergara et al., 2018) (Wagner, 1988b)
D38	Center of wrist crease to root digit 1	From 24 to 39	Y	(Jee and Yun, 2016) (Vergara et al., 2018)
D39	Center of wrist crease to root digit 2	From 24 to 26	Y	(Jee and Yun, 2016) (Vergara et al., 2018)
D40	Center of wrist crease to root digit 3	From 24 to 23	Y	(Jee and Yun, 2016) (Vergara et al., 2018)
D41	Center of wrist crease to root digit 4	From 24 to 29	Y	(Jee and Yun, 2016) (Vergara et al., 2018)
D42	Center of wrist crease to root digit 5	From 24 to 31	Y	(Jee and Yun, 2016) (Vergara et al., 2018)
D43	Digit 1 interphalangeal joint circumference	Across 1, 57, 2, 58	N	(Greiner, 1991) (Jee and Yun, 2016) (García-Cáceres et al., 2012) (Cakit et al., 2014) (GARRETT, 1971) (Nag et al., 2003) (Garrett, 1971) (Vergara et al., 2018) (Robinette and Annis, 1986) (Yu et al., 2013) (Yu et al., 2018)
D44	Digit 2 distal interphalangeal joint circumference	Across 5, 6	N	(Greiner, 1991) (García-Cáceres et al., 2012) (Cakit et al., 2014) (GARRETT, 1971) (Nag et al., 2003) (Garrett, 1971) (Yu et al., 2013) (Yu et al., 2018)
D45	Digit 2 proximal interphalangeal joint circumference	Across 7, 8	N	(Greiner, 1991) (Jee and Yun, 2016) (García-Cáceres et al., 2012) (Cakit et al., 2014) (GARRETT, 1971) (Nag et al., 2003) (Garrett, 1971)
D46	Digit 3 distal interphalangeal joint circumference	Across 9, 10	N	(Greiner, 1991) (García-Cáceres et al., 2012) (Cakit et al., 2014) (GARRETT, 1971) (Nag et al., 2003) (Garrett, 1971) (Yu et al., 2013) (Yu et al., 2018)
D47	Digit 3 proximal interphalangeal joint circumference	Across 12, 11	N	(Greiner, 1991) (Jee and Yun, 2016) (García-Cáceres et al., 2012) (Cakit et al., 2014) (GARRETT, 1971) (Nag et al., 2003) (Garrett, 1971) (Yu et al., 2013)
D48	Digit 4 distal interphalangeal joint circumference	Across 14, 13	N	(Greiner, 1991) (Cakit et al., 2014) (Garrett, 1971) (Yu et al., 2013) (Yu et al., 2018)
D49	Digit 4 proximal interphalangeal joint circumference	Across 16, 15	N	(Greiner, 1991) (Jee and Yun, 2016) (Cakit et al., 2014) (Garrett, 1971) (Yu et al., 2013)
D50	Digit 5 distal interphalangeal joint circumference	Across 18, 17	N	(Greiner, 1991) (Cakit et al., 2014) (Garrett, 1971) (Yu et al., 2013) (Yu et al., 2018)
D51	Digit 5 proximal interphalangeal joint circumference	Across 20, 19	N	(Greiner, 1991) (Jee and Yun, 2016) (García-Cáceres et al., 2012) (Cakit et al., 2014) (Garrett, 1971) (Yu et al., 2013)
D52	Hand circumference	Across 21, 48, 22, 49	N	(Churchill et al., 1978) (Greiner, 1991) (Jee and Yun, 2016) (GARRETT, 1971) (Kar et al., 2003) (Nag et al., 2003) (Stephanidis, 2014) (Chandra et al., 2011) (Garrett, 1971) (Robinette and Annis, 1986) (Yu et al., 2013) (Bures et al., 2016) (Yu et al., 2018) (Robinette et al., 1999)
D53	Wrist circumference	Across 36,24, 37,50	N	(International Organization for Standardization, 2017) (Greiner, 1991) (Jee and Yun, 2016) (García-Cáceres et al., 2012) (Cakit et al., 2014) (GARRETT, 1971) (Garrett, 1971) (Yu et al., 2013) (Yu et al., 2018)

Wrist crease base line: The line crosses landmarks 36 and 37 on the projection plane.

summarizes these landmarks and dimensions, and the references regarding each of them.

To keep the consistency across different measurement methods, some dimensions, such as the breadths and lengths, were measured on a projection plane of the hand as Fig. 3. For projecting the 3D hand on a plane, a local Cartesian coordinate system of the model was defined where the geometric center of the hand was taken as the origin, and the X, Y and Z axes were specified based on the Principal Component Analysis (PCA) analysis (Wold et al., 1987) of all vertices on the model. Most dimensions regarding the breadth and the length of the hand can be calculated as the distance between two projected landmarks, however, with some exceptions. D13, D20, D21, D22, D23, D24, D25, D26, D27 and D28 are the distances from the landmarks on the hand to the wrist crease base line, which can be described as a virtual line crosses landmark 36 and 37. The thickness of the hand was taken as the maximum of the four measured knuckle thicknesses, and the breadth of the interphalangeal joint 1 was measured in the 3D space instead of the projection plane, as in the "standard posture", the thumb tilts slightly regarding the projection plane.

2.2. Using DNN to explore the importance of dimensions

2.2.1. Augment data based on SSM

Though researchers made excessive efforts in recruiting participants

in ergonomics studies, the number of participants is usually limited. In this paper, a 3D human hand SSM is introduced to augment 3D hand models (Yang et al., 2021). The hand SSM (M) consists of a mean model and a set of PCs that describe the shape variations as:

$$M = M_{mean} + \sum_{i=1}^{N_c} \gamma_i PC_i \tag{1}$$

Here M_{mean} represents the mean model of SSM and N_c is the number of PCs ($N_c = 20$ in this study). γ_i is the weight of the corresponding PC_i. Different PCs have different contributions to the model and here we introduce the compactness (Yang et al., 2021) to quantify how efficiently the model describes the total variance in the population. Using 20 PCs with different levels of contributions, the SSM used in this paper can achieve a total of 98% compactness. Regarding the accuracy, the model can fit a 3D scan of a human hand with a root mean square error (RMSE) of 1.21 mm, regardless of the age, weight and height of the subject (Yang et al., 2021).

Using the SSM and based on Eq. (1), a hand model can be augmented as $M = \{(M(\gamma,D)|\gamma = (\gamma_1,\cdots,\gamma_i,\cdots,\gamma_{N_c}), D = \{D_1,\cdots,D_i,\cdots,D_{N_d}\})\}$, where γ is a set of weights within the valid region ($mean(\gamma_i) \pm 3\sigma_i$), D is the set of dimensions that generated based on γ using the method proposed in Section 2.1 and $N_d = 53$, which is the number of dimensions. As each vertex on an augmented 3D model can be considered topologically the same as the corresponding vertex on the mean model, the landmarks specified on the mean model can be mapped to any augmented models, and the dimensions of those models can be computed accordingly based on those mapped landmarks. In this study, 80,000 hand models (M) were augmented based on 80,000 random sets of γ, and the weights (γ) and the generated dimensions (D) are used as the dataset for this study. Fig. 4 (a) presents the mean model of the SSM (in the standard posture). In Fig. 4(b), the dimension D1 of the 80,000 models are presented regarding the randomly generated γ_1 and γ_2, where 4 augmented hand models with different γ_1 and γ_2 are presented as well.

2.2.2. From dimensions to 3D shape by DNN

Using different sets of γ, different 3D hand models can be augmented using the SSM, and subsequently, the dimensions of the hand can be computed based on the landmarks. However, γ cannot be measured, but dimensions can be. The purpose of this step is to build the "inverse" relations of using the SSM to generate dimensions, i.e. to find the relationship from hand dimensions (D) to the 3D hand shape. Due to the complicated geometry, it is difficult to quantify the hand shape with a few parameters in 3D. Therefore, instead of building relations from dimensions to vertices of the hand model directly, we focused on exploring the relation from hand dimensions $D = \{D_1,\cdots,D_i,\cdots,D_{N_d}\}$ to the weight $\gamma = (\gamma_1,\cdots,\gamma_i,\cdots,\gamma_{N_c})$ of PCs used to generate the model. Twenty DNNs with the Multi-Layer Perceptron (MLP) structure were developed to establish such relations, where the inputs of the network are the set of hand dimensions D and the output is the weight coefficient $\gamma_i | \ i = 1...20$ of the hand SSM, respectively. The dataset generated before, which consists of 80,000 hand models with the known weights and the corresponding dimensions, was used to train the DNNs.

As a fully connected network, every neuron in a DNN is connected to all neurons in adjacent layers. Fig. 5(a) illustrates the schematic representation of one of 20 DNNs. In this DNN, the 53 inputs are the 53 hand dimensions, respectively. The output is one of the 20 weights γ_i. In between, there are four hidden layers, which have 150, 200, 200, and 200 neurons, respectively. Based on this structure, the output z_u^k of u_{th} neuron in k_{th} hidden layer of the DNN can be computed as:

$$h_u^k = W^k z^{k-1} + b_u^k = \sum_{t=1}^{Q_{k-1}} \left(W_{tu}^k z_t^{k-1}\right) + b_u^k \tag{2}$$

$$z_u^k = f\left(h_u^k\right) \tag{3}$$

where z^{k-1} is the input of k_{th} layer, and W^k is the weight matrix for the k_{th} layer. W^k consists of the weight W_{tu}^k that indicates the impact strength between t_{th} neuron in the $(k-1)_{th}$ layer and the u_{th} neuron in k_{th} layer. b_u^k is the bias, Q_{k-1} means the number of neurons in the $(k-1)_{th}$ layer where Q_0 is the dimension of the input layer (53 in this paper). The nonlinear performance of the neural network is decided by $f(\cdot)$, which is a nonlinear activation function. In the proposed DNN, the Rectified Linear Unit (ReLU) function was adopted as the activation function.

For training the DNN, a loss function, e.g. mean square errors (MSEs), is often needed for minimizing the difference between the predictions and the known labels. In the proposed research, in order to identify important dimensions among all dimensions for each PC, we adopted the structured sparsity learning method for pruning non-dominant dimensions in the input layer of each DNN (Wen et al., 2016). Given W as all weights in the network, the loss function to be minimized for a K-layer DNN was formulated as:

$$\mathrm{E}(W) = E_D(W) + \lambda \cdot R(W) + \lambda_g \cdot \sum_{k=1}^{K} R_g\left(W^k\right) \tag{4}$$

where $E_D(\cdot)$ represents the MSE term of the network. $R(\cdot)$ stands for the regularization term, which is added to prevent overfitting. λ is the regularization turning parameter, and the $l1$-norm regularization was adopted in this work. $R_g(\cdot)$ is the structured sparsity regularization term on each layer and can be represented as $R_g(W^k) = \sum_{g=1}^{G} w^{(g)}$. Specifically, W^k is a 2D tensors $W^k \in \mathbb{R}^{Q_{k-1} \times Q_k}$, which is the weight matrix of the k_{th} layer. $w^{(g)}$ is a group of weights in W^k, where the group represents the sparsity structure in W^k, i.e. the structure of weights in W^k for sparsity. Technically, the structure could be shape-wise, row-wise, or column-wise (Zhou et al., 2019b), and G is the total number of groups. In this work, the structure is specified as the column-wise structure, therefore G equals to the numbers of neurons in the next layer. In Fig. 5(b), the details of the calculation between the input layer (hand dimensions) and the first hidden layer are shown, and the $w^{(g)}$ is the group of each column (orange or blue) in W^1.

After the training process, the weight pruning process (Wen et al., 2016) was adopted to eliminate the neurons with less contribution. In detail, a $w^{(g)}$ with a significant smaller $l2$-norm value was regarded as a less important group (dash line in Fig. 5(c)), and for a neuron, if all connections between it and the rest of DNN had less important weights, it was regarded as an unimportant neuron (e.g. white neurons in Fig. 5 (c)) and was eliminated from the original trained model. Then the DNN was retrained based on the pruned networks. This process iterated until the model with retained neurons (e.g. blue neurons in Fig. 5(c)) can satisfy the requirement for accuracy (in this paper, 96% accuracy). Finally, input neurons (dimensions) that have significant contributions to this DNN were kept as important dimensions of this PC. More details about this pruning process can be found in (Wen et al., 2016).

Being an important dimension of a PC does not necessarily mean that this dimension is a dominant dimension of the 3D shape, as the contributions of different PCs to the 3D shapes are different. Based on the compactness of each PC and the weights of the identified important dimensions, the dominance of each dimension to the 3D shape can be calculated as:

$$DI_i = \sum_{j=1}^{N_c} d_i^j P_j \tag{5}$$

where DI_i represents the dominance of the i_{th} dimension to the whole SSM and P_j represents the compactness of PC_j. d_i^j means the importance of the i_{th} dimension to PC_j. For a specific PC, d_i can be calculated as:

$$d_i = \frac{L(w^{(g)})_i}{\sum_{g=1}^{G} L(w^{(g)})_g} \tag{6}$$

where $L(\cdot)$ means the $l2$-norm value of the input $(\cdot)$. The larger the importance is, the more the influence it has on the output (Zhou et al., 2019b). With Eq. (5) and Eq. (6), among the union of important dimensions of all PCs, dimensions with dominance $DI_i > 1\%$ were selected as dominant dimensions in this research.

2.3. Measurement comparison

The dominance of each hand dimension is identified in the previous section. In this section, we study the measurement stability of the defined 53 dimensions with the focus on the difference of using different measurement methods. As discussed before, the direct and the indirect method were often used in acquiring anthropometric data, and each has its pros and cons. Therefore, we selected a direct method (Method one, M-I) and an indirect method (Method two, M-II) in the investigation of the measurement variance regarding the hand dimensions. Here M-I is a combination of 2D photography analysis and the traditional direct measuring method and for M-II, a 3D scanner was used to digitize the hand, and dimensions were measured based on the acquired 3D scans.

2.3.1. Participants

A total of 14 volunteers (7 males and 7 females), were invited to the study. Their ages were between 24 and 48 (mean: 28.07 ± 5.84). All subjects were healthy and had no hand-related diseases. Before the experiment, all subjects signed the informed consent to approve the use of measurements in the research. Fifty-three hand dimensions, as specified in Section 2.1, were measured based on the right hand of the participants using M-I and M-II, respectively. The study was approved by the human research ethical committee (HREC) of the Delft University of Technology.

2.3.2. Methods of the measurement

2.3.2.1. Method-I. The first method combines 2D image analysis and the direct measuring method to measure the hand dimensions. A document scanner was used to capture a picture of the hand. Before scanning, an A3 paper with the contour of the standard posture was used to guide the participant to place his/her right hand on the scanner (Fig. 6 (a)), then it was removed for scanning. A printed ruler was scanned simultaneously with the hand to establish relations between pixels and dimensions. Since the lid of the scanner cannot be fully closed during the scanning process, a dark blanket was used to shield the environment light (Fig. 6(b)). A scanning process was often completed within 1 minute and the result was saved as a PDF file with the resolution of 400 dpi. The collected files were analyzed by Inkscape (Bah, 2009) for extracting the needed dimensions (Fig. 6(c)). Dimensions that cannot be acquired from the image, such as the thickness of the hand and circumferences of fingers, were measured by a caliper (the resolution is 0.01 mm) and a self-made tape (Fig. 6(d), the resolution is 1 mm). For each participant, the complete process was repeated five times, and the total time duration was approximately an hour. Finally, the mean of the five measurement values regarding one dimension was taken as the measurement result of this dimension.

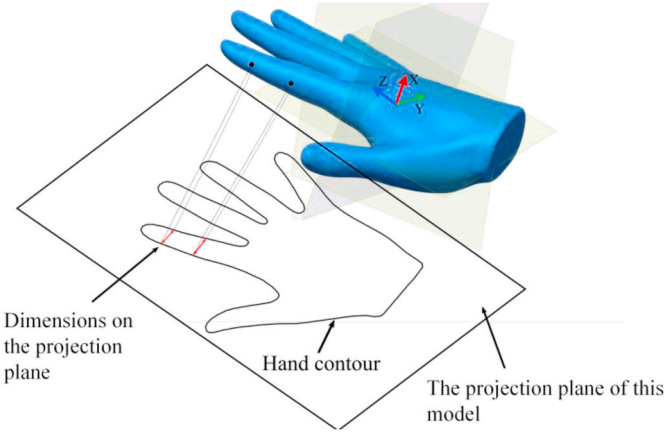

Fig. 3. Measure dimensions using the projected hand contour.

2.3.2.2. Method-II. A scanning system consisting of two Artec Eva® scanners mounted on a rotatory arm was used to capture the 3D model of the hand, as shown in Fig. 7. First, the participant was asked to place the right hand in the depth-of-field of both scanners (Fig. 7(a,b)). Then he/she was instructed to put his/her hand with the "standard posture" and kept the hand steady during scanning. In the data acquisition process, the scanners rotated around the hand while scanning at a speed of 16 frames per second. It took about 10 s to complete the whole scanning process, and the data was stored in a computer and post-processed by the Artec Studio®. Fig. 7(c) presents two examples of the scanning results. Even though all participants were required to put the hand in "standard posture", the posture variances were inevitable among all scans. Therefore, after the 3D scan was obtained, the posture correction algorithm from (Yang et al., 2021) was adopted to align the 3D scan to the "standard posture" to avoid posture variations.

To acquire dimensions from the 3D scans, researchers often select the landmarks via the user interface of the software. This often introduces intra- and inter-observer variations (Kouchi and Mochimaru, 2011), (Kouchi et al., 1999). To minimize the intra- and inter-observer variation, we automated the process by using a model registration method to find the landmarks, and subsequently, the dimensions of each scan. First, the mean model of SSM with the associated landmarks (as described in Section 2.1) was taken as the template model. Then this template was registered to each of the acquired 3D scans using the non-rigid registration method proposed in (Yang et al., 2021). In a registered 3D scan, the vertices that correspond to the template's landmarks were defined as the landmarks of this scan, and the dimensions were then extracted accordingly. Finally, a *t*-test was used to identify the differences between the outcomes of using M-I and M-II. Dimensions that had significant differences were categorized as DHMV, and other dimensions can be described as DLMV.

2.4. 3D hand model approximation from dimensions

In the previous two sections, hand dimensions were evaluated regarding two aspects: 1) the contribution of each dimension to the 3D hand shape, where the dominant dimensions and the non-dominant dimensions were identified; 2) the robustness of the measurement, where the DLMV and DHMV were defined. Though dominant dimensions have large influences on the 3D hand shape, large measurement variance in some of these dimensions may lead to the wrong estimation of the 3D shapes. Therefore, in this step, the intersection of the dominant dimensions and DLMV was highlighted as DDLMV. A new set of DNNs was built to estimate the 3D hand shape based on the DDLMVs. The structure of each DNN was similar to the DNN presented in Section 2.2 except for the inputs, which were the DDLMVs. Besides, the structured sparsity regularization term $(\lambda_g \cdot \sum_{k=1}^{K} R_g(W^k))$ in the loss function was eliminated. The output of the i_{th} DNN in the set was the weight coefficient γ_i of the corresponding PC_i. With all γ_i predicted by the DDLMVs, a 3D hand model can be generated using the SSM.

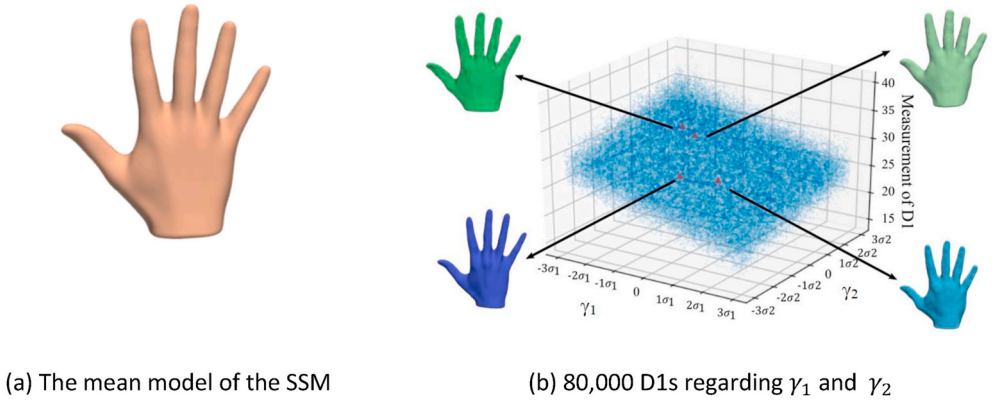

Fig. 4. The SSM and data argumentation.

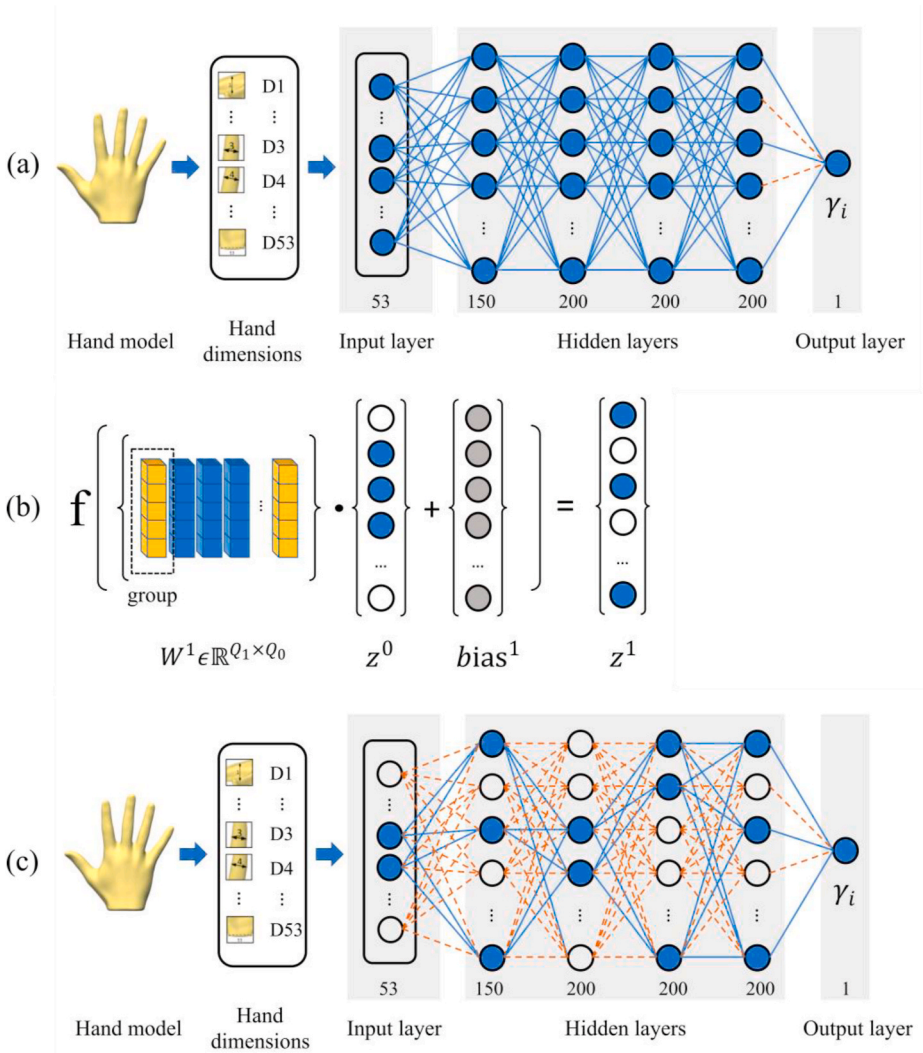

Fig. 5. The schematic representation of the DNN network. (a) The structure of one of the 20 DNNs. The inputs of each DNN are the hand dimensions, and the output is the weight coefficient γ_i. (b) The details of the calculation of the first hidden layer. (c) After a step in the pruning process, the unimportant neurons (white) and the associated link (orange dash lines) will be eliminated, and the DNN will be retrained based on the remaining neurons (blue). (For interpretation of the references to color in this figure legend, the reader is referred to the Web version of this article.)

3. Results

3.1. The importance of dimensions

As proposed in Section 2.2, the importance of each dimension for a PC can be calculated after the network training process. The dimensions that have a large influence on the weight of the corresponding PC can be identified, and other dimensions will be pruned. The importance (d_i^j in Eq. (6)) of each dimension regarding the weights of PCs are presented in Fig. 8. In the figure, each dimension is listed along the horizontal axis and along the vertical axis, each PC is listed. The color of the block stands for the importance of this dimension regarding the weight of the corresponding PC. For example, dimension D9 is the most important dimension (reddest blocks in the figure) for the weights of the first and

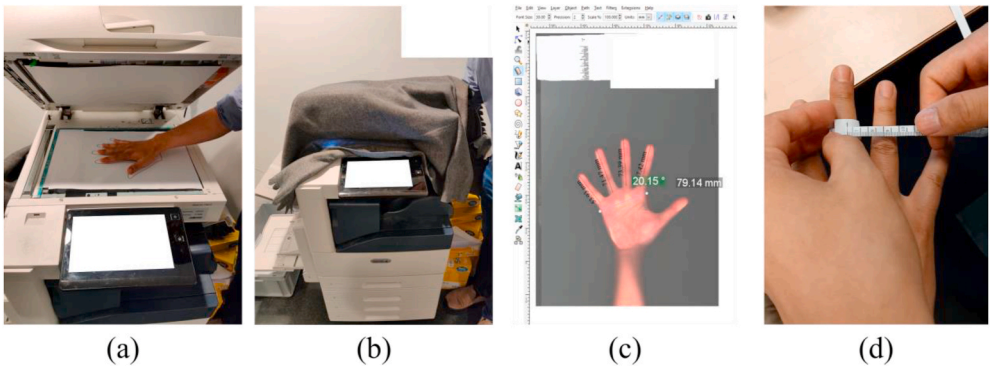

Fig. 6. Use M-I to measure the dimensions of the hand. (a) Place the hand on the document scanner. (b) The scanner was covered by a blanket during scanning. (c) Using Inkscape® to analyze the captured image where the printed ruler is presented on the top. (d) A self-made tape was used to measure the dimensions that cannot be captured by the scanner.

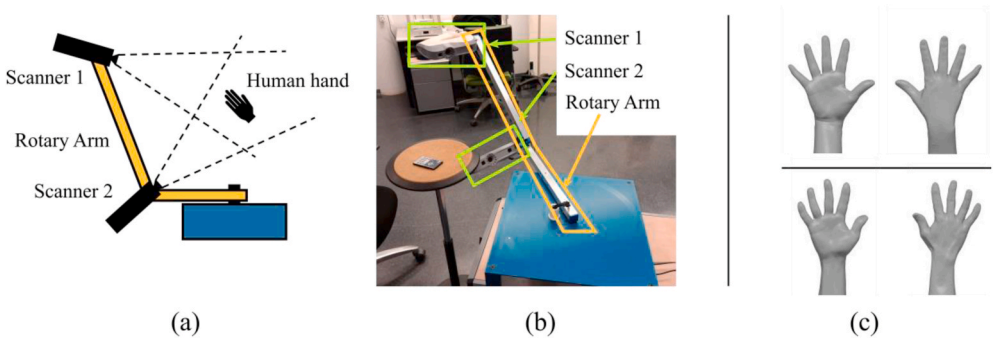

Fig. 7. 3D scanning of human hands. (a) The setup of the 3D scanning system. (b) The scanning system. (c) Two 3D hand models (from both palmar and dorsal sides) that were captured by the scanner.

the second PCs, which takes about 21.8% and 17.4% importance, respectively. Dimension D41 has a larger impact on the weights of PC3 and PC4. It is also noticed that dimension D13 is not important regarding the weights of all PCs, which indicates that it has few influences on the 3D shape.

According to Eq. (5), the dominance is defined on the importance of the dimension regarding a specific PC and the compactness of this PC, and being an important dimension of a PC does not necessarily imply that this dimension is a dominant dimension of the 3D shape. Table 3 lists the compactness of the PCs regarding the selected hand SSM (Yang et al., 2021). Based on Eq. (5), the dominance of each dimension to the whole hand SSM was calculated and illustrated in Fig. 9. In Fig. 9 (a), all dimensions are sorted based on the values of their dominance along the horizontal axis. Dimensions with the dominance value $> 1\%$ were taken as the dominant dimensions for the SSM, and the others were treated as non-dominant dimensions. Twenty-one dominant dimensions were identified. Among them, D9 is the most important dimension for the hand SSM, which accounts for 17.7% of the dominance. The cumulative dominance of all dimensions is shown in Fig. 9(b). Table 3 lists the number of important dimensions regarding each PC, which was selected after weight pruning, and the number of dominant dimensions, which was selected based on Eq. (5) using 1% as a threshold.

3.2. The measuring variations of dimensions

All dimensions were measured by M-I and M-II, respectively, and a *t*-test was used to compare the differences between these two methods. The mean and the standard deviation of the measured hand dimensions for all participants are shown in Table 4. It can be found that for most dimensions, the standard deviation of M-I is larger or equal to the standard deviation of M-II, except D2, D3, D4, D7, D8, D9, D10, D11. Among the 53 dimensions, 45 had no significant difference ($p > 0.05$) between the uses of these two measuring methods, but there were significant differences ($p < 0.05$) regarding the measurement results of 8 dimensions: D15, D28, D30, D32, D34, D36, D37, D49. The 45 dimensions were treated as DLMVs, and the eight dimensions were categorized as DHMVs. It is worth mentioning that most measurement values of DHMV (7 out of 8) captured by M-II are significantly smaller than the measurement values of Method-I, except dimension D37, which is the length of the medial phalanx link of Digit 5.

3.3. 3D model approximation based on DDLMVs

Based on the discovered dominant dimensions and the DLMV, 16 DDLMVs can be identified by removing 5 DHMVs from the 21 dominant dimensions. The DDLMVs are D9, D10, D39, D3, D12, D11, D8, D14, D22, D7, D33, D41, D43, D4, D2 and D20. The sequence of this list was sorted according to the dominance of each dimension. Fig. 10(a) presents all dominant dimensions, and 16 DDLMVs are colored with blue. In Fig. 10(b), the dominant dimensions, DHMVs, and DDLMVs are summarized in the same table. Furthermore, the DDLMVs regarding each PC are given as well. For different PCs, the kept dimensions are different. It can be found that for PC6 and PC13, they are influenced by the largest number of DDLMVs (15), and for PC5 and PC19, only 10 DDLMVs were identified. Regarding each DDLMV, D9 contributed to 16 PCs except PC4, PC11, PC17 and PC20.

Using the augmented data and the DNN construction methods presented in Section 2.4, we built and trained three models to predict the 3D hand shape based on three sets of dimensions (Set 1: all dimensions; Set 2: 21 dominant dimensions; Set 3: 16 DDLMVs). Each model has a set of DNNs where the inputs are the dimension set, the outputs are $(\gamma_1, \cdots, \gamma_i, \cdots, \gamma_{N_c})$. Using these three models, we predicted each 3D hand shape based

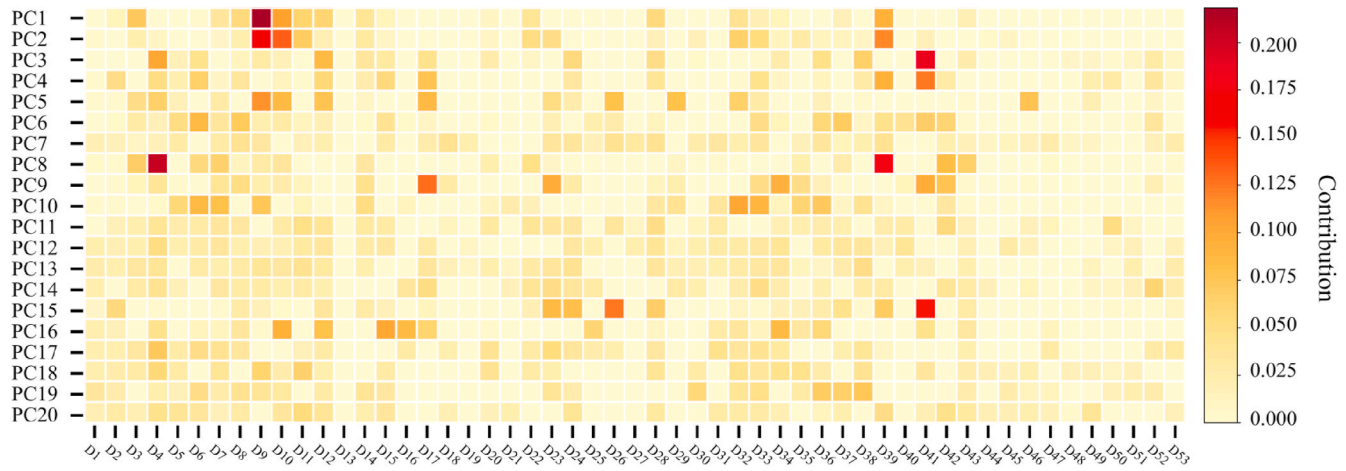

Fig. 8. The contribution of dimensions regarding the weights of each principal component.

Table 3
Important and dominant dimensions regarding PCs.

	PC1	PC2	PC3	PC4	PC5	PC6	PC7	PC8	PC9	PC10
Compactness	0.6969	0.1098	0.0741	0.0270	0.0150	0.0132	0.0082	0.0069	0.0054	0.0048
Number of important dimensions	20	27	28	27	23	32	39	22	28	26
Number of dominant dimensions	19	19	15	15	11	19	15	13	15	15
	PC11	PC12	PC13	PC14	PC15	PC16	PC17	PC18	PC19	PC20
Compactness	0.0040	0.0036	0.0033	0.0028	0.0025	0.0020	0.0019	0.0017	0.0013	0.0013
Number of important dimensions	34	37	37	34	29	24	30	31	28	35
Number of dominant dimensions	17	18	19	14	18	15	16	17	13	19

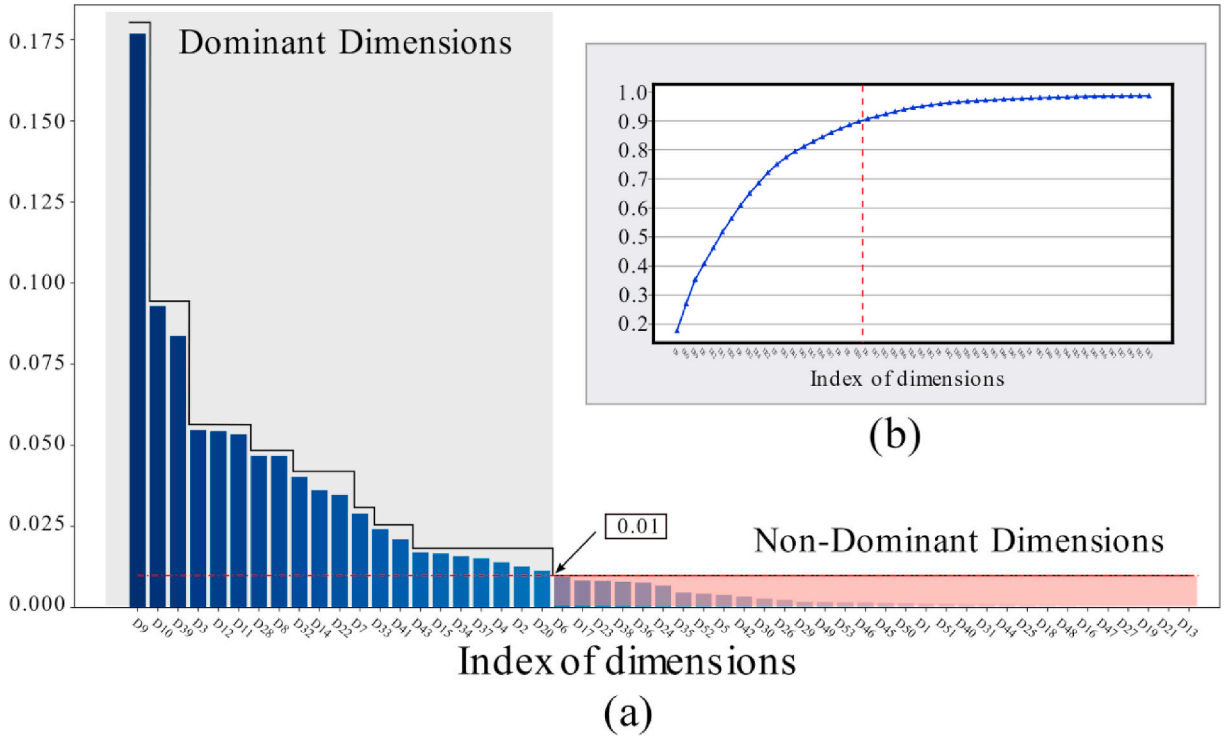

Fig. 9. Identify dominant dimensions.

on measurements collected using M-I and M-II, respectively. The RMSEs between the predicted 3D hands and the corresponding 3D scans regarding each participant are presented in Tables 5 and 3 typical scans (~P5, ~P50, ~P90) are presented in Fig. 11. When all dimensions were used to approximate the 3D model, the average RMSEs were 9.2 mm and 3.0 mm regarding using the collected data from M-I and M-II, respectively. With only dominant dimensions, the average RMSEs increased to 9.5 mm and 8.1 mm, and using the selected 16 DDLMVs, the average

Table 4
Hand Dimensions of the 14 participants acquired by the two measurement methods.

Dimension	M-I (mm)	M-II (mm)	P value	Dimension	M-I (mm)	M-II (mm)	P value
D1	25.5 ± 2.7	25.7 ± 2.5	0.84	**D28**[a]	138.3 ± 16.9	124.6 ± 12.4	***0.03***
D2	20.5 ± 2.4	20.5 ± 3.0	1.00	**D29**	29.5 ± 2.8	27.9 ± 2.3	0.14
D3	16.8 ± 1.7	16.7 ± 2.0	0.97	**D30**[a]	24.5 ± 2.9	21.6 ± 1.7	***0.00***
D4	19.0 ± 1.9	19.6 ± 2.1	0.43	**D31**	21.6 ± 3.1	20.8 ± 1.2	0.40
D5	16.7 ± 1.5	16.1 ± 1.5	0.40	**D32**[a]	25.0 ± 3.0	22.7 ± 1.9	***0.03***
D6	19.0 ± 1.8	18.5 ± 1.8	0.54	**D33**	24.9 ± 3.3	26.0 ± 1.6	0.29
D7	15.8 ± 1.6	15.2 ± 1.7	0.34	**D34**[a]	25.1 ± 2.9	22.1 ± 2.2	***0.01***
D8	17.6 ± 1.8	17.8 ± 1.9	0.80	**D35**	22.4 ± 2.0	22.9 ± 1.5	0.44
D9	14.7 ± 1.6	13.7 ± 1.9	0.17	**D36**[a]	23.0 ± 2.6	20.0 ± 2.2	***0.00***
D10	16.1 ± 1.5	15.5 ± 2.0	0.42	**D37**[a]	16.0 ± 1.9	17.4 ± 1.4	***0.04***
D11	85.0 ± 6.2	87.6 ± 6.8	0.33	**D38**	68.8 ± 6.6	70.8 ± 6.3	0.44
D12	55.8 ± 6.1	55.7 ± 5.1	0.94	**D39**	105.0 ± 9.6	103.7 ± 8.4	0.71
D13	106.5 ± 9.9	105.3 ± 8.9	0.74	**D40**	106.3 ± 10.0	100.4 ± 8.1	0.11
D14	35.3 ± 2.4	37.0 ± 2.0	0.06	**D41**	103.0 ± 9.9	100.0 ± 7.9	0.41
D15[a]	58.4 ± 6.0	52.3 ± 4.0	***0.01***	**D42**	96.0 ± 9.4	90.8 ± 7.2	0.12
D16	70.0 ± 5.4	66.4 ± 3.8	0.06	**D43**	63.6 ± 7.0	64.6 ± 6.7	0.71
D17	76.7 ± 5.7	77.7 ± 5.1	0.65	**D44**	50.9 ± 5.0	53.6 ± 2.2	0.08
D18	71.8 ± 5.5	68.9 ± 5.2	0.17	**D45**	61.2 ± 6.7	64.8 ± 2.4	0.08
D19	57.3 ± 4.9	55.6 ± 4.8	0.40	**D46**	51.4 ± 5.3	53.7 ± 1.7	0.13
D20	62.7 ± 6.6	67.6 ± 6.9	0.08	**D47**	61.6 ± 6.7	64.3 ± 2.3	0.18
D21	103.9 ± 9.5	104.7 ± 9.3	0.82	**D48**	48.1 ± 5.0	50.5 ± 1.7	0.11
D22	104.2 ± 10.3	102.8 ± 9.3	0.72	**D49**[a]	57.6 ± 6.8	50.5 ± 1.7	***0.00***
D23	93.1 ± 10.5	89.0 ± 8.9	0.28	**D50**	44.2 ± 4.7	44.4 ± 2.5	0.93
D24	90.2 ± 8.8	94.1 ± 8.3	0.25	**D51**	51.2 ± 5.3	52.4 ± 2.9	0.48
D25	169.5 ± 13.2	174.2 ± 12.5	0.36	**D52**	196.2 ± 16.2	193.4 ± 15.0	0.65
D26	182.4 ± 15.3	181.1 ± 13.9	0.82	**D53**	161.6 ± 16.4	154.6 ± 13.4	0.24
D27	170.9 ± 16.5	164.8 ± 14.0	0.32				

[a] The dimensions with higher measurement variance.

RMSEs were 5.9 mm and 3.4 mm for using dimensions collected from M-I and M-II, respectively.

4. Discussion

The aim of this study is to identify the dominant dimensions that influence the 3D hand shape and to analyze the measurement stability of those dimensions regarding different measuring methods. Based on the discovered 16 DDLMVs, we also explored the opportunity of building 3D hand models directly from these measurements. In the following, we discuss our findings regarding the dimensions, the measurement methods and the approach.

4.1. The dominant dimensions

Fig. 8 illustrates that there are 21 dominant dimensions that have more than 1% dominance. The first two dominant dimensions are D9, D10, which are the breadths of the distal interphalangeal and proximal interphalangeal joints of digit 5 (pinky finger). They account for 17.7% and 9.3% dominance of the hand shape, respectively. As both of them are the measures of the pinky finger, the absolute values of these two dimensions are relatively small, and it is suggested that extra attention should be paid in measuring these two dimensions.

Almost all dominant dimensions are related to breadths and lengths of different parts of the hand, except the dimension D43, which is the circumference of the digit 1 interphalangeal joint. The reason behind this might be that the circumference is strongly correlated to the corresponding breadth. This finding is in accordance with the literature (Greiner, 1991) where the circumference can be approximated by a function defined on the breadth of the joint. Moreover, over half of the dominant dimensions are hand-finger-related dimensions, which indicates that the shape of fingers has a significant influence on the hand shape.

Jee and Yun (2016) defined 27 hand dimensions and found that 78.3% of the variances of the hand dimensions can be described by three major factors: the hand breadth, the palm length and the finger length. Compared those 27 dimensions to the proposed 21 dominant dimensions, half of them are identical, such as the finger joint breadths (D10, D8, D4), wrist breadth (D12), and the lengths from the center of the wrist to the finger roots (D41, D39). Even though fewer dimensions are listed, the proposed 21 dominant dimensions can represent 90% of the shape variance. The reason might be that some dominant dimensions (e.g. D14 and D20) were not enlisted in (Jee and Yun, 2016). Additionally, some highly correlated dimensions were included in the result of (Jee and Yun, 2016), e.g. the finger joint circumference and the finger breadth, which may also be redundant for building the set of dominant dimensions.

4.2. The measurement methods

Two methods were introduced in the measurement of human hands. Using M-I, data can be collected with simple instruments. However, large intra- and inter-observer variations are often observed (Kouchi et al., 1999). Using M-II, with the hand template and the non-rigid registration method proposed in (Yang et al., 2021), intra- and inter-observer variations can be minimized. However, it is more expensive than using M-I regarding manpower, computing power and equipment. The result of the *t*-test (Table 4) indicated that measurement results of 8 dimensions (D15, D28, D30, D32, D34, D36, D37, D49) were significantly different regarding the use of measurement methods. A possible explanation for this is that: 1) in the use of M-I, despite that the participants were guided to position their hands to the "standard posture" before the scanning process, slight deviations were inevitable (e.g. D28); 2) the deformation of the soft tissues was inevitable when participants placed their hand on the photocopier (e.g. D15) and 3) for short distance without clear landmarks, e.g. D32, D34, D37, the percentages of inter- and intra-observer variations over the length are higher than the dimensions with clear landmarks and relatively longer length.

4.3. The DDLMVs

Based on the ideal measurements of dominant dimensions of the augmented data, the 3D shape of the hand can be accurately

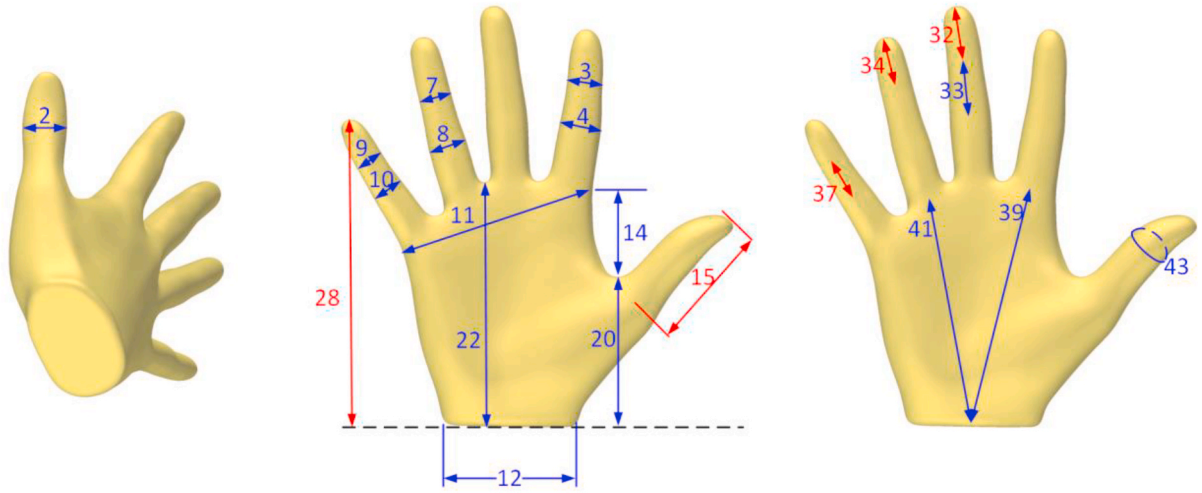

(a) 21 dominant dimensions. the DDLMVs (16) are colored by blue, the rest (5) are in red.

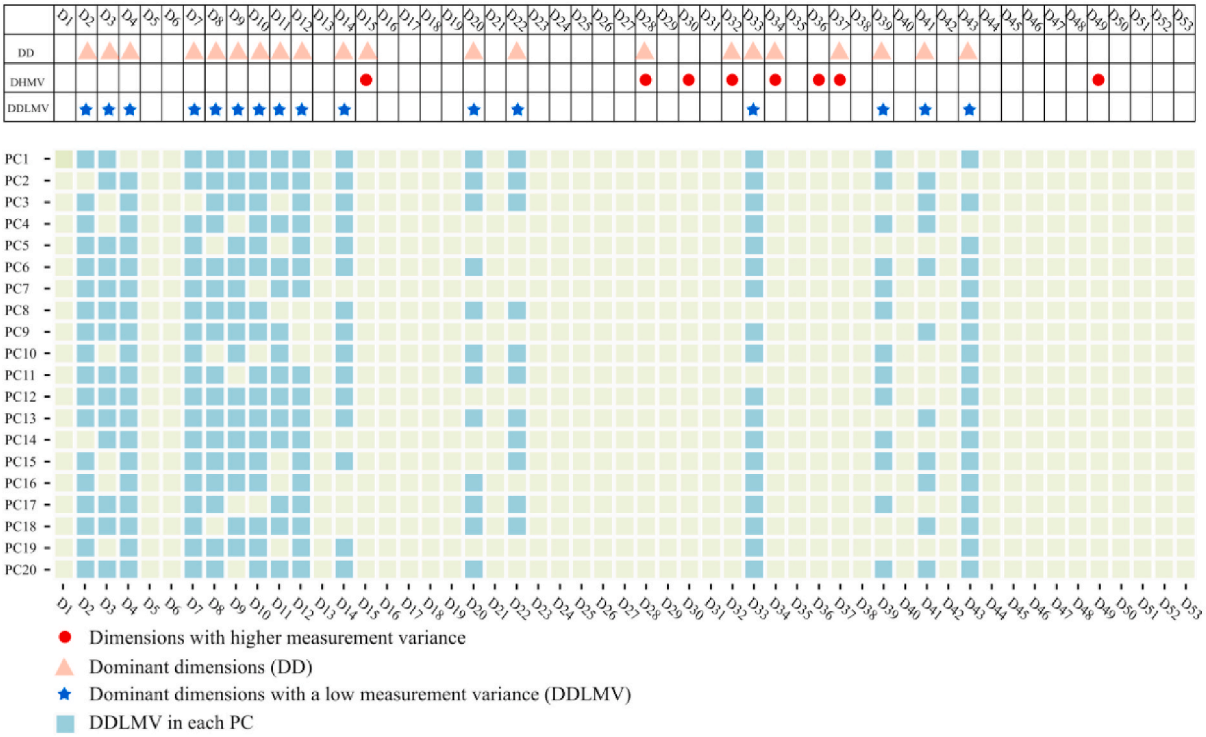

(b) Different dimension sets and the DDLMVs for each PC.

Fig. 10. The identified DDLMVs.

approximated using DNNs. However, in practical scenarios, the measurement errors may lead to large deviations. In this research, based on the analysis of robustness of the measurements, we proposed a set of 16 dimensions named DDLMVs. To verify the effectiveness of this set of dimensions, we construct 3 models that can infer 3D shapes from all dimensions, dominant dimensions and DDLMVs, respectively. The RMSEs (Table 5) proved that pruning those non-dominant dimensions does not affect the accuracy of the reconstructed 3D model, and the measurement errors might lead to larger reconstruction errors. For instance, after removing the DHMV from dominant dimensions, though fewer dimensions were used, the accuracy of the reconstructed 3D models increased, e.g. the mean RMSEs dropped from 9.5 mm to 5.9 mm, and from 8.1 to 3.4 mm regarding using data collected from M-I and M-II, respectively.

4.4. Potential applications

Since most shape information of the human hand can be represented by the proposed 21 dominant dimensions, those dimensions are suggested as the recommend dimensions for hand anthropometric study and hand-related product design. Collecting more hand dimensions can indeed describe more properties of the hand shape. However, more efforts are needed in the data acquisition process.

Though measurement results indicated that using M-II was more

Table 5
Reconstruction Error (RMSE, in mm).

Sample index	All dimensions		21 dominant dimensions		16 DDLMVs	
	Method-I	Method-II	Method-I	Method-II	Method-I	Method-II
1	14.2	3.2	16.5	13.0	4.6	3.8
2	12.7	2.9	14.7	9.4	11.1	3.1
3	7.9	2.3	10.2	8.0	5.7	3.3
4	7.6	1.8	7.3	9.0	5.2	2.9
5	13.0	2.4	8.7	4.4	9.2	3.3
6	7.0	4.8	6.1	7.2	7.9	3.7
7	5.3	1.8	9.6	9.9	3.6	3.1
8	6.2	1.5	11.0	9.0	3.8	2.2
9	5.7	1.8	4.3	2.7	3.9	2.1
10	13.3	6.6	8.4	12.7	4.7	3.3
11	10.9	3.4	9.3	7.9	4.1	3.6
12	10.9	2.7	7.3	5.6	5.7	4.8
13	9.5	4.2	10.1	7.5	9.6	4.9
14	4.7	2.9	10.0	7.5	3.0	3.8
Mean	9.2 ± 3.16	3.0 ± 1.35	9.5 ± 3.04	8.1 ± 2.70	5.9 ± 2.46	3.4 ± 0.77

accurate than using M-I, using M-I was more convenient regarding the needed manpower, computing power and equipment. Among all 16 DDLMVs, 15 can be acquired from a 2D image of the hand from the palmar aspect and D2 can be measured by a caliper. Due to the wide availability of cameras, this finding offers an easy, effective and efficient way of generating 3D models for ergonomics study and product design, especially in the early stage of the design. For instance, in the personalized product design application, a customer can be involved in the early stage of the design process by providing these 16 DDLMVs for a better fit of the glove, or hand tools.

4.5. The approach

In this research, we introduced a novel approach that synthesizes the computational methods and the traditional measurement methods to explore the importance of different anthropometric measures. In the use of the computational methods, a valid and accurate SSM of the 3D shape and the use of DNN with the structured sparsity learning method are the keys. The SSM used in this research was developed by (Yang et al., 2021), and it is able to fit a 3D hand scan with an accuracy of 1.21 mm. In the construction of the DNN, there is no strict requirement for the structure of the DNN, but the MLP structure is recommended due to its simplicity. Utilizing the structured sparsity learning method during the training process to recognize the importance of each input neuron is essential in this step. Based on the effectiveness of the proposed DDLMVs, it could be inferred that the proposed approach can be generalized to other studies, which brings a tool for researchers in finding dominant dimensions that influence 3D shapes.

4.6. Limitations

Even though we synthesized 53 dimensions in this study, most of them were measured from the palmar aspect. As indicated by Vergara et al. (2018), significant differences can be found for some dimensions that are measured from the dorsal and palmar aspects, respectively. There is a possibility that some dimensions from the dorsal aspect, which may be important to the hand shape, are not considered in this study. In the future, more comprehensive dimensions defined from both dorsal and palmar aspects will be explored. Another limitation of this study is that, even though the dimensions of a 3D hand model are measured on a projected plane, there is a small difference compared to measuring those dimensions using an image collected by the document scanner. The reason is that the shape and the deformation of the soft tissue in the palm may influence the contact area between the palm and the glass in the document scanner. Though we use PCA to compute the hand projection plane, it is an approximation and the "real" planes might be different among individuals. Besides, in the process of exploring measurement stability, we only compared two methods with a limited number of participants. More measurement methods, with more participants and researchers with different backgrounds, will be conducted in the future.

5. Conclusions

This study investigated the importance of different hand dimensions regarding the 3D shape and proposed 21 dominant dimensions, where 16 of them were further refined as DDLMVs. Experiment results indicated that these 16 dimensions represent 90% variance of the 3D hand shape and are able to generate 3D shapes with an RMSE of 5.9 mm using traditional measurement methods. These findings suggest a prioritized list of dimensions for ergonomists in the anthropometric study of the human hand and a potentially easy way to construct 3D hand shapes based on the 16 DDLMVs, as nearly all of them can be acquired based on a 2D image of the hand. Though the accuracy is limited, the generated 3D models can be used as an indicator for different applications, especially in the early stage of research/design. Besides, the proposed approach can also be generalized to other ergonomics studies on finding critical factors that influence 3D shapes.

Declaration of competing interest

The authors declare that they have no known competing financial

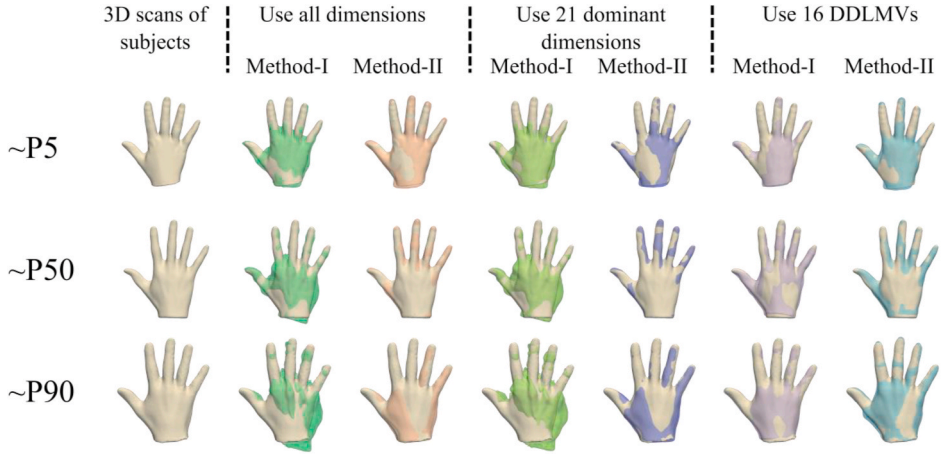

Fig. 11. Comparing 3D scans and the reconstructed 3D hands using 3 sets of measurements from M-I and M-II.

interests or personal relationships that could have appeared to influence the work reported in this paper.

Acknowledgment

The work of Mr. Yusheng Yang is sponsored by the China Scholarship Council (CSC, No. 201806890056). The work of Mr. Hongpeng Zhou is sponsored by the China Scholarship Council (CSC, No.201706120017). The authors of this paper would like to express their sincere appreciation to Dr. Johan F. M. Molenbroek, Dr. Toon Huysmans, Dr. Willemijn S. Elkhuizen, Mr. Jun Xu, Ms. Tianyun Yuan, Ms. Tessa T. W. Essers, Mr. Bertus J. Naagen, Mr. Adrie Kooijman and Mr. Martin Verwaal for the fruitful discussions and kind assistance during the experiment.

References

Ahn, S.H., Kwon, S., Bahn, S., Yun, M.H., Yu, W., 2016. Effects of grip curvature and hand anthropometry for the unimanual operation of touchscreen handheld devices. Hum. Factors Ergon. Manuf. 26 (3), 367–380. https://doi.org/10.1002/hfm.20662.

Bah, T., 2009. Inkscape: Guide to a Vector Drawing Program (Digital Short Cut), vol. 14. Pearson.

Bayraktar, N.K., Özşahin, E., 2018. "Anthropometric measurement of the hand," *East.* J. Med. 23 (4), 298–301. https://doi.org/10.5505/ejm.2018.03164.

Bennett, K.A., Osborne, R.H., 1986. Interobserver measurement reliability in anthropometry. Hum. Biol. 58 (5), 751–759.

Bishop, C.M., 2006. Pattern Recognition and Machine Learning. Springer.

Bures, M., Gorner, T., Sediva, B., 2016. Hand anthropometry of Czech population. IEEE Int. Conf. Ind. Eng. Eng. Manag. 2016, 1077–1082. https://doi.org/10.1109/IEEM.2015.7385814.

Cakit, E., Durgun, B., Cetik, O., Yoldas, O., 2006. A survey of hand anthropometry and biomechanical measurements of dentistry students in Turkey. Hum. Factors Ergon. Manuf. 16 (1), 61–81. https://doi.org/10.1002/hfm.

Cakit, E., Durgun, B., Cetik, O., Yoldas, O., 2014. A survey of hand anthropometry and biomechanical measurements of dentistry students in Turkey. Hum. Factors Ergon. Manuf. Serv. Ind. 24 (6), 739–753, 10.1002/hfm.

Chandra, A., Chandna, P., Deswal, S., 2011. Analysis of hand anthropometric dimensions of male industrial workers of Haryana state. Int. J. Eng. 5 (3), 242–256.

Cheng, Y., Wang, D., Zhou, P., Zhang, T., 2017. A Survey of Model Compression and Acceleration for Deep Neural Networks, pp. 1–10. " arXiv. arXiv:1710.09282.

Chuan, T.K., Hartono, M., Kumar, N., 2010a. Anthropometry of the Singaporean and Indonesian populations. Int. J. Ind. Ergon. 40 (6), 757–766. https://doi.org/10.1016/j.ergon.2010.05.001.

Chuan, T.K., Hartono, M., Kumar, N., 2010b. Anthropometry of the Singaporean and Indonesian populations. Int. J. Ind. Ergon. 40 (6), 757–766. https://doi.org/10.1016/j.ergon.2010.05.001.

Churchill, E., Laubach, L.L., McConville, J.T., Tebbetts, I., 1978. Anthropometric Source Book Volume I: Anthropometry for Designers, vol. I.

Dewangan, K.N., Owary, C., Datta, R.K., 2008. Anthropometric data of female farm workers from north eastern India and design of hand tools of the hilly region. Int. J. Ind. Ergon. 38 (1), 90–100. https://doi.org/10.1016/j.ergon.2007.09.004.

García-Cáceres, R.G., Felknor, S., Córdoba, J.E., Caballero, J.P., Barrero, L.H., 2012. Hand anthropometry of the Colombian floriculture workers of the Bogota plateau. Int. J. Ind. Ergon. 42 (2), 183–198. https://doi.org/10.1016/j.ergon.2011.12.002.

Garrett, J.W., 1971b. The adult human hand. Some anthropometric and biomechanical considerations. Hum. Factors 13 (2), 117–131. https://doi.org/10.1177/001872087101300204.

Garrett, J., 1971. Anthropometry of the hands of male Air Force flight personnel. Appl. Ergon. 2 (4), 244. https://doi.org/10.1016/0003-6870(71)90118-9.

Greiner, T.M., 1991. Hand anthropometry of U.S. Army personnel. Tech. Rep. Natick 434. TR-92/011, no. December 1990. http://oai.dtic.mil/oai/oai?verb=getRecord&metadataPrefix=html&identifier=ADA244533 [Online]. Available:

Harih, G., Dolšak, B., Jul. 2013. Tool-handle design based on a digital human hand model. Int. J. Ind. Ergon. 43 (4), 288–295. https://doi.org/10.1016/j.ergon.2013.05.002.

Harih, G., Dolšak, B., 2014. Comparison of subjective comfort ratings between anatomically shaped and cylindrical handles. Appl. Ergon. 45 (4), 943–954. https://doi.org/10.1016/j.apergo.2013.11.011.

Hertzberg, H.T.E., 1912. The conference on standardization of anthropometric techniques and terminology, pp. 1–16.

Hochreiter, S., Urgen Schmidhuber, J., 1997. Long shortterm memory. Neural Comput. 9 (8), 17351780.

Imrhan, S.N., Nguyen, M.-T., Nguyen, N.-N., Dec. 1993. Hand anthropometry of Americans of Vietnamese origin. Int. J. Ind. Ergon. 12 (4), 281–287. https://doi.org/10.1016/0169-8141(93)90098-X.

Imrhan, S.N., Sarder, M.D., Mandahawi, N., 2009. Hand anthropometry in Bangladeshis living in America and comparisons with other populations. Ergonomics 52 (8), 987–998. https://doi.org/10.1080/00140130902792478.

International Organization for Standardization, 2017. ISO 7250-1:2017 Basic human body measurements for technological design - Part 1: Body measurement definitions and landmarks. International Organization for Standardization.

Jee, S.C., Yun, M.H., 2016. An anthropometric survey of Korean hand and hand shape types. Int. J. Ind. Ergon. 53, 10–18. https://doi.org/10.1016/j.ergon.2015.10.004.

Kanchan, T., Krishan, K., 2011. Anthropometry of hand in sex determination of dismembered remains - a review of literature. J. Forensic Leg. Med. 18 (1), 14–17. https://doi.org/10.1016/j.jflm.2010.11.013.

Kar, S.K., Ghosh, S., Manna, I., Banerjee, S., Dhara, P., 2003. An investigation of hand anthropometry of agricultural workers. J. Hum. Ecol. 14 (1), 57–62. https://doi.org/10.1080/09709274.2003.11905598.

Khadem, M.M., Islam, M.A., 2014a. Development of anthropometric data for Bangladeshi male population. Int. J. Ind. Ergon. 44 (3), 407–412. https://doi.org/10.1016/j.ergon.2014.01.007.

Khadem, M.M., Islam, M.A., 2014b. Development of anthropometric data for Bangladeshi male population. Int. J. Ind. Ergon. 44 (3), 407–412. https://doi.org/10.1016/j.ergon.2014.01.007.

Klamklay, J., Sungkhapong, A., Yodpijit, N., Patterson, P.E., 2008. Anthropometry of the southern Thai population. Int. J. Ind. Ergon. 38 (1), 111–118. https://doi.org/10.1016/j.ergon.2007.09.001.

Kouchi, M., Mochimaru, M., 2011. Errors in landmarking and the evaluation of the accuracy of traditional and 3D anthropometry. Appl. Ergon. 42 (3), 518–527. https://doi.org/10.1016/j.apergo.2010.09.011.

Kouchi, M., Mochimaru, M., Tsuzuki, K., Yokoi, T., 1999. Interobserver errors in anthropometry. J. Hum. Ergol. 28 (1–2), 15–24. https://doi.org/10.11183/jhe1972.28.15.

Krizhevsky, A., Sutskever, I., Hinton, G.E., 2012. ImageNet classification with deep convolutional neural networks. Handb. Approx. Algorithms Metaheuristics 1–1432. https://doi.org/10.1201/9781420010749.

Mandahawi, N., Imrhan, S., Al-Shobaki, S., Sarder, B., 2008. Hand anthropometry survey for the Jordanian population. Int. J. Ind. Ergon. 38 (11–12), 966–976. https://doi.org/10.1016/j.ergon.2008.01.010.

Nag, A., Nag, P.K., Desai, H., 2003. Hand anthropometry of Indian women. Indian J. Med. Res. 117, 260–269. https://doi.org/10.1016/j.biotechadv.2011.08.021 (Secreted).

Nasa, 1978. Anthropometric source book volume I: anthropometry for designers, I (2), 1–606. https://doi.org/10.1007/s13398-014-0173-7.2.

Okunribido, O.O., 2000. A survey of hand anthropometry of female rural farm workers in ibadan, western Nigeria. Ergonomics 43 (2), 282–292. https://doi.org/10.1080/001401300184611.

Ozsoy, U., Demirel, B.M., Yildirim, F.B., Tosun, O., 2009. "Method Selection in Craniofacial Measurements: Advantages and Disadvantages of 3D Digitization Method, pp. 285–290. https://doi.org/10.1016/j.jcms.2008.12.005.

Patel, T., Ningthoujam, B., Kumar, P., Gurung, S., 2018. Validation of two-dimensional digital photogrammetry measurement for hand anthropometric dimensions. J. Ergon. https://doi.org/10.4172/2165-7556.1000236, 04.

Prado-León, L.R., Avila-Chaurand, R., González-Muñoz, E.L., 2001. Anthropometric study of Mexican primary school children. Appl. Ergon. 32 (4), 339–345. https://doi.org/10.1016/S0003-6870(01)00009-6.

Rhiu, I., Kim, W., 2019. Estimation of stature from finger and phalange lengths in a Korean adolescent. J. Physiol. Anthropol. 38 (1), 1–8. https://doi.org/10.1186/s40101-019-0206-1.

Richardson, F., Member, S., Reynolds, D., Dehak, N., 2015. Deep neural network approaches to speaker and language recognition, 22 (10), 1671–1675.

Robinette, K., Annis, J., 1986. A Nine-Size System for Chemical Defense Gloves. Defense Technical Information Center.

Robinette, K.M., Daanen, H., Paquet, E., 1999. The CAESAR project: a 3-D surface anthropometry survey. In: Second International Conference on 3-D Digital Imaging and Modeling. No. PR00062, pp. 380–386. Cat.

Robinette, K., et al., 1991. Civilian American and European surface anthropometry resource (ceasar). SAE Int. 5. December.

Shahriar, M.M., Parvez, M.S., Lutfi, M., Jul. 2020. A survey of hand anthropometry of Bangladeshi agricultural farm workers. Int. J. Ind. Ergon. 78 https://doi.org/10.1016/j.ergon.2020.102978, 102978.

Sjöberg, J., Hjalmarsson, H., Ljung, L., 1994. Neural networks in system identification. IFAC Proc 27 (8), 359–382. https://doi.org/10.1016/s1474-6670(17)47737-8.

Stellon, M., Seils, D., Mauro, C., 2017. Assessing the importance of surgeon hand anthropometry on the design of medical devices. J. Med. Devices, Trans. ASME 11 (4), 1–6. https://doi.org/10.1115/1.4037257.

Stephanidis, C., 2014. "3D hand anthropometry of Korean teenager's and comparison with manual method. Commun. Comput. Inf. Sci. 435 https://doi.org/10.1007/978-3-319-07854-0. PART I, no. June.

Vergara, M., Agost, M.J., Gracia-Ibáñez, V., 2018. Dorsal and palmar aspect dimensions of hand anthropometry for designing hand tools and protections. Hum. Factors Ergon. Manuf. 28 (1), 17–28. https://doi.org/10.1002/hfm.20714.

Wagner, C., 1988a. "The pianist's hand: anthropometry and biomechanics. Ergonomics 31 (1), 97–131. https://doi.org/10.1080/00140138808966651.

C. Wagner, "The pianist's hand: anthropometry and biomechanics," Ergonomics, vol. 31, no. 1, pp. 97–131, Jan. 1988, doi: 10.1080/00140138808966651.

Wen, W., Wu, C., Wang, Y., Chen, Y., Li, H., 2016. Learning structured sparsity in deep neural networks. Adv. Neural Inf. Process. Syst. 2082–2090.

Wold, S., Esbensen, K.I.M., Geladi, P., 1987. Principal component analysis, 2, 37–52.

Yang, Y., Yuan, T., Huysmans, T., Elkhuizen, W.S., Tajdari, F., Song, Y., 2021. Posture-invariant 3D human hand statistical shape model. J. Comput. Inf. Sci. Eng. 21 (3) https://doi.org/10.1115/1.4049445.

Yu, A., Yick, K.L., Ng, S.P., Yip, J., May 2013. 2D and 3D anatomical analyses of hand dimensions for custom-made gloves. Appl. Ergon. 44 (3), 381–392. https://doi.org/10.1016/J.APERGO.2012.10.001.

Yu, A., Yick, K.L., Ng, S.P., Yip, J., March 2018. Case study on the effects of fit and material of sports gloves on hand performance. Appl. Ergon. 75, 17–26. https://doi.org/10.1016/j.apergo.2018.09.007, 2019.

Zhou, H., Ibrahim, C., Pan, W., 2019a. A Sparse Bayesin Deep Learning Approach for Identificaiton of Cascaded Tanks Benchmark. " arXiv:1911.06847, no. 2017.

Zhou, H., Yang, M., Wang, J., Pan, W., 2019b. "Bayesnas: a bayesian approach for neural architecture search," in *36th international Conference on machine learning*. ICML 13116–13140, 2019.